INTERNATIONAL JOURNAL FOR NUMERICAL METHODS IN FLUIDS, VOL. 21, 1049–1066 (1995)

SPURIOUS NUMERICAL REFRACTION

B. CATHERS

Department of Civil and Mining Engineering, University of Wollongong, Northfields Avenue, New South Wales 2522, Australia

AND

S. BATES

British Gas Corporation, Engineering Research Station, Harvey Combe, Killingworth, PO Box 1LH, Newcastle upon Tyne NE99 1LH, U.K.

SUMMARY

The purpose of this paper is to investigate the effect of a non-uniform mesh in two dimensions (2D). A change in mesh size will, in general, result in spurious refraction (and reflection) which is entirely numerical (rather than physical) in origin. To facilitate the analysis, the mesh geometry has been highly simplified in that only a single change in mesh size is considered. The analysis is based on a finite element wave model.

The domain consists of two conterminous regions discernible only by their different nodal spacings in the x-direction. The interface between the two regions is internal to the mesh and is a straight line. The model is based upon the Crank–Nicolson linear finite element scheme applied to the second order wave equation. The results of the analysis are confirmed by numerical experiments. It is shown that under particular numerical conditions total internal reflection may occur and when this is the case, the transmitted wave is evanescent. An analysis of the energy flux associated with the incident, reflected and transmitted waves shows that energy is conserved across the interface between the two regions.

KEYWORDS: spurious wave refraction; total internal reflection

1. INTRODUCTION

An appreciation of the effects of a non-uniform mesh is fundamental to a good understanding of the processes occurring in numerical models with varying mesh sizes. This is particularly relevant to time dependent finite element (FE) models and interactively nested finite difference (FD) models (in contradistinction to passively nested FD models). Practioners are often faced with questions such as 'how much can I change the mesh size and what are the consequences?'

In 1D linear systems, these questions have been partly addressed.[1–3] The analyses were completed for the simplified situation of a 1D domain consisting of two semi-infinite regions abutting at a common interfacial node. The two regions were discernible on numerical grounds (e.g. different mesh spacings or different numerical algorithms) or physical grounds (effected by an abrupt change in coefficient in the governing equation). The latter case is not considered herein and hence the inclusion of the word 'spurious' in the title of the present paper.

The magnitude of the effects of a change in 1D mesh size were quantified by determining the amplitudes of the transmitted and (unwanted) reflected waves, and their associated energy fluxes due to an incident wave. In a more general sense, the incident wave may be interpreted as one of many Fourier components which can be superimposed to make up a general waveform.

In 1D, a change in mesh size results in both *wave reflection* and *wave transmission*. In 2D however, there is an additional process at work viz *wave refraction*. The interface between the two conterminous

CCC 0271–2091/95/111049–18

Received October 1994
Revised April 1995

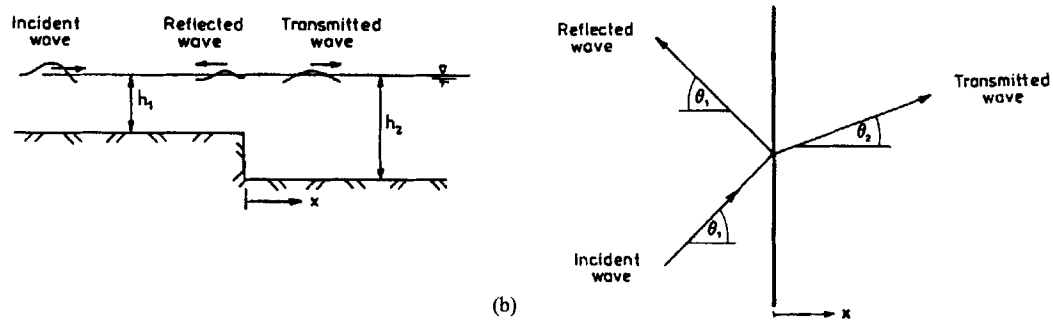

Figure 1. (a) Section and (b) plan view of an incident wave impinging on an abrupt change in depth giving rise to a reflected wave and a transmitted wave

regions is a straight line, and incident waves impinging upon the interface give rise to a reflected wave and a transmitted wave. The incident wave is refracted as it passes into the downstream region. It will also be shown that under particular *numerical* conditions total internal reflection (TIR) can occur–obviously an undesirable result.

Since the algebra for the analysis quickly becomes lengthy, two major simplifications have been made. Firstly, the present paper is concerned with the relatively simple, lumped 2D FE 'wave equation' scheme with Crank–Nicolson finite differencing in time. This is a linear system in which superposition is valid. In a non-linear system, superposition would not hold and small wavelengths would be continually generated by the non-linear terms, especially at any discontinuities.

Secondly, the FE mesh has a regular geometry. Although it is two dimensional, only a single, abrupt change in mesh size is considered together with a straight line interface. An irregular interface would result in a confused wave field and render the analysis intractable. However, the wave processes of reflection and refraction would still be present. Finite element meshes used in engineering practice would normally (i) be graded, (ii) vary in all directions and (iii) have irregularly shaped elements.

Before proceeding with the analysis for the discrete system, it is instructive to first consider a parallel case in the continuum in which the wave reflection, refraction and transmission are necessarily effected by physical means. In this case, the only difference between the upstream region (referred to as region 1) and the downstream region (i.e. region 2) are the mean depths (Figure 1).

2. GOVERNING EQUATIONS

2.1. *Continuum*

The analysis of wave behaviour in the continuum is based upon the linear shallow water equations

$$\frac{\partial u}{\partial t} + g\frac{\partial \eta}{\partial x} = 0, \tag{1}$$

$$\frac{\partial v}{\partial t} + g\frac{\partial \eta}{\partial y} = 0, \tag{2}$$

$$\frac{\partial \eta}{\partial t} + h\frac{\partial u}{\partial x} + h\frac{\partial v}{\partial y} = 0, \tag{3}$$

where (u, v) are the (x, y) velocity components, η is the surface elevation above mean water level, h is the mean depth which is constant and g is the acceleration due to gravity. Equations (1) and (2) are the x- and y-momentum equations and equation (3) is the continuity equation.

The shallow water equations are used here in preference to the second order wave equation in order to facilitate enforcing the internal boundary conditions across the interface. If it is assumed that the velocities (u, v) vary sinusoidally in time with angular frequency ω, it can be shown from equations (1) and (2) that

$$u = \left(\frac{ig}{\omega}\right)\frac{\partial \eta}{\partial x}, \tag{4}$$

$$v = \left(\frac{ig}{\omega}\right)\frac{\partial \eta}{\partial y}. \tag{5}$$

The dispersion relation for the continuum is found by substituting equations (4), (5) and the solution for a unit amplitude wave, $\eta = \exp[i(\omega t - \sigma_x x - \sigma_y y)]$ into equation (3) giving

$$\omega = \pm \sigma c, \tag{6}$$

where $\sigma = \sqrt{\sigma_x^2 + \sigma_y^2}$ and $c = \sqrt{gh}$.

2.2. *Discrete System*

The analysis of wave behaviour in the discrete system is based upon the second order wave equation. The wave equation is obtained by taking the x-derivative of equation (1), the y-derivative of equation (2), the time derivative of equation (3) and eliminating all mixed derivatives.

$$\frac{\partial^2 \eta}{\partial t^2} - c^2\left(\frac{\partial^2 \eta}{\partial x^2} + \frac{\partial^2 \eta}{\partial y^2}\right) = 0. \tag{7}$$

The dispersion relation for the discrete system is determined in a later section.

3. REFRACTION IN THE CONTINUUM

The waves present are the incident wave which gives rise to a reflected wave and a transmitted wave (Figure 1). In region 1, the surface elevation is the result of a unit incident wave with wavenumber components $(\sigma_{x1}, \sigma_{y1})$ and a reflected wave with amplitude β and wavenumber components $(-\sigma_{x1}, \sigma_{y1})$.

$$\eta_1 = e^{i(\omega t - \sigma_{x1} x - \sigma_{y1} y)} + \beta e^{i(\omega t + \sigma_{x1} x - \sigma_{y1} y)} \tag{8}$$

Using equations (4), (5) and (8), the velocity components in the upstream region (u_1, v_1) can be determined as

$$u_1 = \left(\frac{g\sigma_{x1}}{\omega}\right)\{e^{i(\omega t - \sigma_{x1} x - \sigma_{y1} y)} - \beta e^{i(\omega t + \sigma_{x1} x - \sigma_{y1} y)}\}, \tag{9}$$

$$v_1 = \left(\frac{g\sigma_{y1}}{\omega}\right)\left\{e^{i(\omega t-\sigma_{x1}x-\sigma_{y1}y)} + \beta e^{i(\omega t+\sigma_{x1}x-\sigma_{y1}y)}\right\}. \tag{10}$$

Similarly, in the downstream region the surface elevation is determined by the transmitted wave with wavenumber components (σ_{x2}, σ_{y2}) and velocity components (u_2, v_2).

$$\eta_2 = \tau e^{i(\omega t-\sigma_{x2}x-\sigma_{y2}y)}, \tag{11}$$

$$u_2 = \left(\frac{g\sigma_{x2}}{\omega}\right)\tau e^{i(\omega t-\sigma_{x2}x-\sigma_{y2}y)}, \tag{12}$$

$$v_2 = \left(\frac{g\sigma_{y2}}{\omega}\right)\tau e^{i(\omega t-\sigma_{x2}x-\sigma_{y2}y)}. \tag{13}$$

Enforcement of the internal boundary conditions along the interface ($x = 0$) permits the solution for the four unknowns σ_{x2}, σ_{y2}, β and τ. The parameters ω, σ_{x1} and σ_{y1} are known.

Mass flow balance and continuity of pressure (and hence surface elevation) across the interface at $x = 0$ requires (for all times and for all y)

$$u_1 h_1 = u_2 h_2, \tag{14}$$

$$\eta_1 = \eta_2. \tag{15}$$

Substitution of equations (8), (9), (11) and (12) into (14) and (15) yields

$$\sigma_{y2} = \sigma_{y1} \quad \text{(Snell's law)} \tag{16}$$

$$= \sigma_y \quad \text{(say)}, \tag{17}$$

$$\beta = \frac{h_1\sigma_{x1} - h_2\sigma_{x2}}{h_1\sigma_{x1} + h_2\sigma_{x2}}, \tag{18}$$

$$\tau = \frac{2h_1\sigma_{x1}}{h_1\sigma_{x1} + h_2\sigma_{x2}}. \tag{19}$$

$$= 1 + \beta. \tag{20}$$

Since the system is linear, the same angular frequency is applicable to both regions and σ_{x2} can be found from the kinematic relation

$$\omega = c_1\sigma_1 = c_2\sigma_2, \tag{21}$$

where $c_1 = \sqrt{gh_1}$ and $c = \sqrt{gh_2}$. That is

$$c_1\sqrt{\sigma_{x1}^2 + \sigma_y^2} = c_2\sqrt{\sigma_{x2}^2 + \sigma_y^2}. \tag{22}$$

This completes the definition of the system of reflected and transmitted waves. The conditions for the occurrence of TIR can be determined from an examination of (i) the angles which the incident and transmitted wave trains make with the positive x-axis, viz θ_1 and θ_2 and (ii) the magnitude of the

reflection coefficient, $|\beta|$.

$$\tan\theta_1 = \frac{\sigma_{y1}}{\sigma_{x1}} = \frac{\sigma_y}{\sqrt{\sigma_1^2 - \sigma_y^2}}, \tag{23}$$

$$\tan\theta_2 = \frac{\sigma_{y2}}{\sigma_{x2}} = \frac{\sigma_y}{\sqrt{\sigma_2^2 - \sigma_y^2}}, \tag{24}$$

where use has been made of Snell's law. When $h_1 < h_2$, $c_1 < c_2$ and equation (21) requires $\sigma_1 > \sigma_2$. From equations (23) and (24), $\theta_1 < \theta_2$ and the transmitted wave is refracted towards the interface. At the critical condition, the transmitted wave is refracted *along* the interface and in this case

$$\theta_2 = \frac{1}{2}\pi, \quad \theta_1 = (\theta_1)_{\text{crit}}, \quad \sigma_{x2} = 0, \quad \sigma_2 = \sigma_y.$$

When $\theta_1 > (\theta_1)_{\text{crit}}$, $\sigma_y > \sigma_2$ and

$$\sigma_{x2} = \pm i\sqrt{\sigma_y^2 - \sigma_2^2}, \tag{25}$$

where σ_{x2} is pure imaginary. Substituting equation (25) into (18) yields $|\beta| = 1$ indicating TIR. By requiring finite surface elevation at $x = \infty$, the positive sign in equation (25) is discarded. Substituting equation (25) into equation (11) gives the resulting surface elevation as

$$\begin{aligned} \eta_2 &= \tau\eta e^{i(\omega t - \sigma_y y)} e^{-i\sigma_{x2}x} \\ &= \tau\eta e^{i(\omega t - \sigma_y y)} e^{-\sqrt{\sigma_y^2 - \sigma_2^2}x}. \end{aligned} \tag{26}$$

Moving in the positive x direction, η_2 is damped in space by the factor $e^{-\sqrt{\sigma_y^2 - \sigma_2^2}x}$.

4. REFRACTION IN THE DISCRETE SYSTEM

In the *discrete* numerical system, the two conterminous regions are discernible on numerical rather than physical grounds; that is by their different mesh spacings, rather than different depths as for the continuum case. The effects however, are similar.

4.1. Dispersion relation

The spatial discretisation of equation (7) was effected through the application of the lumped mass, Galerkin FE technique using linear, rectangular finite elements ($\Delta x \times \Delta y$) and lumped mass matrix.

$$\begin{aligned} 6s\left(\frac{\Delta x \Delta y}{c^2}\right)\left(\frac{\partial^2\eta}{\partial t^2}\right)^n_{j,k} &= -8(s^2+1)\eta^n_{j,k} \\ &\quad + (s^2+1)[\eta_{j-1,k-1} + \eta_{j+1,k-1} + \eta_{j+1,k+1} + \eta_{j-1,k+1}]^n \\ &\quad + 2(2s^2-1)[\eta_{j+1,k} + \eta_{j-1,k}]^n - 2(s^2-2)[\eta_{j,k+1} + \eta_{j,k-1}]^n = 0 \end{aligned} \tag{27}$$

where Δx, Δy, Δt are the discrete step sizes in space (x, y) and time (t); j, k, n are the indices indicating the node position ($j\Delta x$, $k\Delta y$) and time $t = n\Delta t$ and $s = \Delta y/\Delta x =$ mesh aspect ratio.

The second order time derivative in (27) will be approximated with a centred finite difference

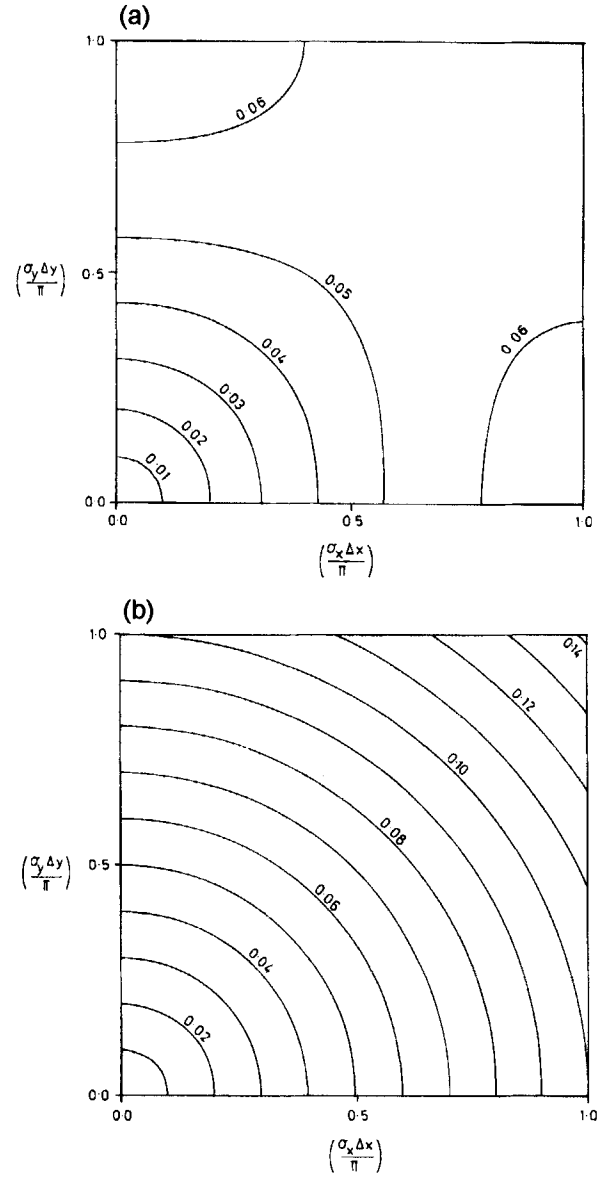

Figure 2. Dispersion relations for (a) the discrete system and (b) the continuum. Contours are for $\omega\Delta t/\pi$. Conditions $C_x = 1/10$; $\Delta y/\Delta x = 1$

formula, viz

$$\left(\frac{\partial^2 \eta}{\partial t^2}\right)^n_{j,k} \approx \frac{(\eta^{n+1} - 2\eta^n + \eta^{n-1})_{j,k}}{\Delta t^2} \tag{28}$$

The dispersion relation for a mesh with nodal spacings Δx and Δy in the x and y directions, is found by substituting a solution of the form

$$\eta^n_{j,k} = e^{i(\omega n \Delta t - j\sigma \Delta x \cos\theta - k\sigma \Delta y \sin\theta)} \tag{29}$$

into equation (27). The dispersion relation for the 2D discrete system is found to be

$$\sin^2\left(\frac{\omega.\Delta t}{2}\right) = \frac{C_x C_y}{6s}[(s^2+1)(2-\cos\gamma_x\cos_y) - (2s^2-1)\cos\gamma_x + (s^2-2)\cos\gamma_y], \tag{30}$$

where $(\gamma_x, \gamma_y) = (\sigma\Delta x \cos\theta, \sigma\Delta y \sin\theta)$ and the Courant numbers are defined as $(C_x, C_y) = (c\Delta t/\Delta x, c\Delta t/\Delta y)$.

The dispersion relations corresponding to waves moving in the positive x-direction for both the discrete system (6) and the continuum (30) are plotted in Figure 2a and b respectively. For the discrete system plot, the conditions are: square mesh (i.e. $\Delta x = \Delta y$) and $C_x = C_y = 0{\cdot}1$.

4.2. Discrete equations

In the numerical refraction analysis which follows, the domain consists of two regions with different but regular grids. The interface between the two regions is defined along $x = 0$ and marks the boundary between two different step lengths in the x direction (see Figure 3a).

Region 1 is characterized by finite elements of size $(\Delta x_1 \times \Delta y)$ and region 2 by elements of size $(\Delta x_2 \times \Delta y)$. The change in mesh size between the two regions is quantified by the parameter $r = \Delta x_2/\Delta x_1$. Thus $r > 1$ represents a mesh expansion in the x-direction and vice versa for a mesh contraction.

To simplify the algebra, the finite elements in region 1 are taken to be squares (i.e. $\Delta x_1 = \Delta y$). Setting $s = 1$ or $s = 1/r$ in equation (27) gives the FE analogues of equation (7) to the left or right of the junction respectively. At the junction, application of the FE technique leads to

$$\begin{aligned}
&\frac{\Delta y}{2}(\Delta x_1 + \Delta x_2)\left(\frac{\partial^2\eta}{\partial t^2}\right)^n_{j,k} \\
&\quad + \frac{c^2}{6}\left(\frac{\Delta y}{\Delta x_1}\right)(-4\eta_{j-1,k} - \eta_{j-1,k+1} + \eta_{j,k+1} + 4\eta_{j,k} - \eta_{j-1,k-1} + \eta_{j,k-1})^n \\
&\quad + \frac{c^2}{6}\left(\frac{\Delta y}{\Delta x_2}\right)(\eta_{j,k+1} + 4\eta_{j,k} - \eta_{j+1,k+1} - 4\eta_{j+1,k} + \eta_{j,k\,1} - \eta_{j+1,k-1})^n \\
&\quad + \frac{c^2}{6}\left(\frac{\Delta x_1}{\Delta y}\right)(2\eta_{j-1,k} - \eta_{j-1,k+1} - 2\eta_{j,k+1} + 4\eta_{j,k} - \eta_{j-1,k-1} - 2\eta_{j,k-1})^n \\
&\quad + \frac{c^2}{6}\left(\frac{\Delta x_2}{\Delta y}\right)(-2\eta_{j,k+1} + 4\eta_{j,k} - \eta_{j+1,k+1} + 2\eta_{j+1k} - 2\eta_{j,k-1} - \eta_{j+1,k-1})^n = 0.
\end{aligned} \tag{31}$$

Substituting equation (28) and $r = \Delta x_2/\Delta x_1$ into equation (31) gives

$$\begin{aligned}
&\left(\frac{\Delta y^2}{2c^2}\right)(1+r)\frac{(\eta^{n+1} - 2\eta^n + \eta^{n-1})_{j,k}}{\Delta t^2} \\
&\quad + \tfrac{1}{6}(-4\eta_{j-1,k} - \eta_{j-1,k+1} + \eta_{j,k+1} + 4\eta_{j,k} - \eta_{j-1,k-1} + \eta_{j,k-1})^n \\
&\quad + \frac{1}{6r}(\eta_{j,k+1} + 4\eta_{j,k} - \eta_{j+1,k+1} - 4\eta_{j+1,k} + \eta_{j,k-1} - \eta_{j+1,k-1})^n \\
&\quad + \tfrac{1}{6}(2\eta_{j-1,k} - \eta_{j-1,k+1} - 2\eta_{j,k+1} + 4\eta_{j,k} - \eta_{j-1,k-1} - 2\eta_{j,k-1})^n \\
&\quad + \frac{r}{6}(-2\eta_{j,k+1} + 4\eta_{j,k} - \eta_{j+1,k+1} + 2\eta_{j+1,k} - 2\eta_{j,k-1} - \eta_{j+1,k-1})^n = 0.
\end{aligned} \tag{32}$$

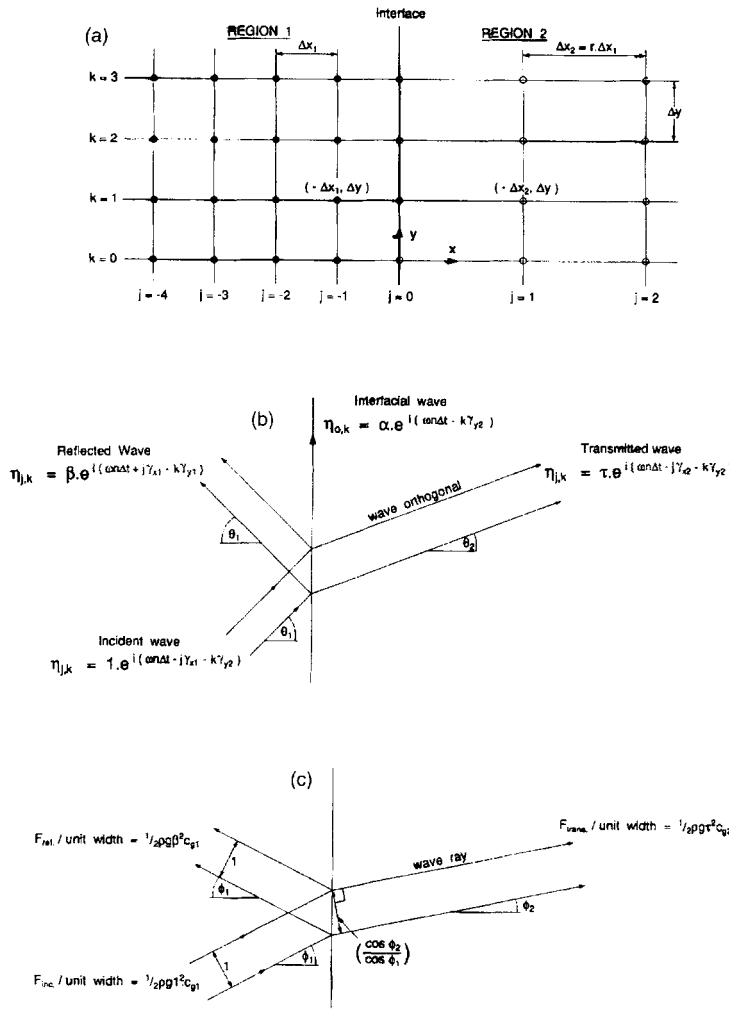

Figure 3. (a) Finite element mesh, (b) wave orthogonals and (c) wave rays

4.3. *Refraction analysis*

For wave-like solutions (29) disturbed by a discontinuity in a regular grid, the unit amplitude incident wave in region 1 is assumed to give rise to a reflected wave (with amplitude β) and a transmitted wave (amplitude τ). It is also assumed that a wave is formed along the interface between the two boundaries (at $x=j=0$) with amplitude α. The solution in the two regions and along the interface is given by

$$\eta^n_{j,k} = e^{i(\omega n\Delta t - j\gamma_{x1} - k\gamma_{y1})} + \beta e^{i(\omega n\Delta t + j\gamma_{x1} - k\gamma_{y1})} \quad \text{for } j \leqslant 0, \tag{33}$$

$$= \alpha e^{i(\omega n\Delta t - k\gamma_{y2})} \quad \text{for } j = 0, \tag{34}$$

$$= \tau e^{i(\omega n\Delta t - j\gamma_{x2} - k\gamma_{y2})} \quad \text{for } j \geqslant 0, \tag{35}$$

where $(\gamma_{x1}, \gamma_{y1}) = (\sigma_1 \Delta x_1 \cos\theta_1, \sigma_1 \Delta y_1 \sin\theta_1)$ and $(\gamma_{x2}, \gamma_{y2}) = (\sigma_2 \Delta x_2 \cos\theta_2, \sigma_2 \Delta y_2 \sin\theta_2)$. The known parameters in equations (33) to (35) are ω, σ_1 and θ_1; the five unknown parameters are α, β, τ, σ_2 and θ_2.

The assumed solutions in equations (33) to (35) need to be compatible at the interface $x = 0$ for all times and for all values of $y = k\Delta y$. As a result, equations (33) to (35) yield

$$1 + \beta = \alpha \tag{36}$$

$$= \tau, \tag{37}$$

$$\gamma_{y1} = \gamma_{y2} \quad \text{(Snell's law)} \tag{38}$$

$$= \gamma_y \quad \text{say.} \tag{39}$$

The dispersion relation applicable to each of the two regions can be found from equation (30) by substituting the appropriate values for C_x, C_y, γ_x, γ_y and s. For region 1, the dispersion relation (with $s = 1$) is

$$\sin^2\left(\frac{\omega \Delta t}{2}\right) = \frac{C_{x1} C_y}{6}(4 - 2\cos\gamma_{x1}\cos\gamma_y - \cos\gamma_{x1} - \cos\gamma_y). \tag{40}$$

The dispersion relation for the downstream region 2 (with $s = 1/r$) is

$$\sin^2\left(\frac{\omega \cdot \Delta t}{2}\right) = \frac{C_{x2} C_y}{6}\left[\left(\frac{1}{r^2} + 1\right)(2 - \cos\gamma_{x2}\cos\gamma_y) - \left(\frac{2}{r^2} - 1\right)\cos\gamma_{x2} + \left(\frac{1}{r^2} - 2\right)\cos\gamma_y\right]. \tag{41}$$

Being a linear system, the wave frequency (ω) associated with the reflected and transmitted waves is unchanged from that of the incident wave. Equations (40) and (41) can be combined to eliminate the angular frequency ω and yield an expression for γ_{x2} (which includes the two unknowns θ_2 and σ_2)

$$\cos\gamma_{x2} = \frac{2 - \cos\gamma_{x1} - 2/r^2 - \cos\gamma_y(2\cos\gamma_{x1} + 1/r^2 - 1)}{(1 - 2/r^2) - \cos\gamma_y(1/r^2 + 1)} \tag{42}$$

$$= R \quad \text{(say)}, \tag{43}$$

where equations (38) and (39) have been used. Equation (42) relates the wave number in region 2 to that in region 1.

The amplitudes α, β and τ may be found from equation (32) after substituting equations (33) to (41). After a great deal of algebraic manipulation the results are

$$\beta = \frac{B - A\sin\gamma_{x2}}{B + A\sin\gamma_{x2}}, \tag{44}$$

$$\tau = \frac{2B}{B + A\sin\gamma_{x2}}, \tag{45}$$

where

$$A = (1/r + r)\cos\gamma_y + (2/r - r), \tag{46}$$

$$B = (1 + 2\cos\gamma_y)\sin\gamma_{x1}. \tag{47}$$

For very long incident wavelengths (L_1), it can be shown that equations (45) and (44) simplify to $\tau \approx 1$ and $\beta \approx 1$ respectively. This can be shown using Taylor series expansions as follows.

As L_1 becomes very large, γ_{x1} and γ_y become very small. Taylor series expansions then yield the following approximations:

$$\cos(\gamma_{x1}) \approx 1 - 0{\cdot}5\gamma_{x1}^2, \tag{48}$$

$$\cos(\gamma_y) \approx 1 - 0{\cdot}5\gamma_y^2. \tag{49}$$

When equations (48) and (49) are substituted into equation (42), the result is

$$\cos(\gamma_{x2}) \approx 1 - \frac{r^2\gamma_{x1}^2}{2} \tag{50}$$

and substitution of equations (48) to (50) into equation (45) leads to the result that $\tau \approx 1$. Equation (37) results in $\beta \approx 1$. The physical interpretation of this result is that the very long waves are relatively unaffected by the change in mesh spacing.

4.4. Occurrence of total internal reflection

It is evident from equations (44) and (45) that provided γ_{x2} is real, the reflection and transmission coefficients are also real. (It will be assumed herein that γ_{x1} and γ_y, which refer to the incident wave, are real. A complex value would correspond to an incident wave which is exponentially decaying or growing in space.)

Inspection of equation (42) shows that although the right-hand side (R) is always real, γ_{x2} need not be real. Whenever the right hand side exceeds unity, γ_{x2} is complex and can be represented by

$$\gamma_{x2} = (\gamma_{x2})_r + i(\gamma_{x2})_i. \tag{51}$$

Taking the cosine of equation (51) and incorporating equation (43) gives

$$\cos(\gamma_{x2}) = \cos(\gamma_{x2})_r \cosh(\gamma_{x2})_i - i\sin(\gamma_{x2})_r \sinh(\gamma_{x2})_i \tag{52}$$

$$= R. \tag{53}$$

Equating the real and imaginary parts yields two solutions for $(\gamma_{x2})_r$ and $(\gamma_{x2})_i$ and hence γ_{x2}

$$\gamma_{x2} = \pi + i\cosh^{-1}(-R) \quad \text{for } R < -1, \tag{54}$$

$$\gamma_{x2} = 0 + i\cosh^{-1}(R) \quad \text{for } R > 1. \tag{55}$$

When $R < -1$ the reflection and transmission coefficients corresponding to γ_{x2} in equation (54) can be found from equations (44) and (45)

$$\beta = \frac{B + iA\sinh[\cosh^{-1}(-R)]}{B - iA\sinh[\cosh^{-1}(-R)]}, \tag{56}$$

$$\tau = \frac{2B}{B - iA\sinh[\cosh^{-1}(-R)]}. \tag{57}$$

When the dimensionless wavenumber in region 2 is $\gamma_{x2} = \pi + i\cosh^{-1}(-R)$ (say), the solution in the two regions is

$$\eta_{j,k} = e^{i(\omega n\Delta t - j\gamma_{x1} - k\gamma_y)} + \beta e^{i(\omega n\Delta t + j\gamma_{x1} - k\gamma_y)} \quad \text{for } j \leqslant 0, \tag{58}$$

$$= \tau e^{i(\omega n\Delta t - j\pi - k\gamma_y)} e^{j\cosh^{-1}(-R)} \quad \text{for } j \geqslant 0, \tag{59}$$

where $e^{j\cosh^{-1}(-R)}$ is the spatial damping factor in the x-direction of the $2\Delta x_2$ transmitted wave in the x-direction.

When $R > 1$ similar expressions for β and τ can be found corresponding to the value of γ_{x2} when determined by equation (55). Of interest is equation (56) from which it is clear that whenever γ_{x2} is complex, $|\beta| = 1$. This corresponds to TIR. Figure 4a, b contains the magnitudes of the reflection coefficient from equations (44) and (56) for $\Delta x_2/\Delta x_1 = 1/2$ and 2 respectively.

It is obviously of value to determine the conditions under which TIR occurs. By examining the conditions under which the right hand side of equation (42) exceeds unity, the 2D domains of γ_{x1} and γ_y ($0 \leqslant \gamma_{x1} \leqslant \pi$, $0 \leqslant \gamma_y \leqslant \pi$) for the incident wave which lead to TIR, can be established. Figure 5a, b indicates the regions of γ_{x1} and γ_y which result in complex γ_{x2} when $\Delta x_2/\Delta x_1 = 1/2$ and 2. It is interesting that TIR can occur for both mesh expansion and mesh contraction in the x-direction.

4.5. Energy balance across the interface

The group velocity defines the rate at which energy is conveyed by a wave. Application of the concept of group velocity to 1D numerical schemes has been well documented[4,6–10] and the theory is easily extended to account for two dimensions. The components of the group velocity vector are

$$\vec{c_g} = (c_{gx}, c_{gy})$$

$$= \left(\frac{\partial\omega}{\partial\sigma_x}, \frac{\partial\omega}{\partial\sigma_y}\right). \tag{60}$$

Differentiating equation (30) with respect to σ_x and σ_y leads to

$$\sin^2(\omega\Delta t)c_{gx} = \left(\frac{C_x C_y}{3}\right)\left(\frac{\Delta x}{\Delta t}\right)\sin\gamma_x\left[\left(s + \frac{1}{s}\right)\cos\gamma_y + 2s - \frac{1}{s}\right], \tag{61}$$

$$\sin^2(\omega\Delta t)c_{gy} = \left(\frac{C_x C_y}{3}\right)\left(\frac{\Delta y}{\Delta t}\right)\sin\gamma_y\left[\left(s + \frac{1}{s}\right)\cos\gamma_x + \frac{2}{s} - s\right], \tag{62}$$

$$\tan\phi = s\frac{\sin\gamma_y[(s + 1/s)\cos\gamma_x + 2/s - s]}{\sin\gamma_x[(s + 1/s)\cos\gamma_y + 2s - 1/s]},$$

where ϕ is the angle the group velocity vector $\vec{c_g}$ makes with the x-axis. Note that whereas the wave orthogonal is perpendicular to the wave crest and is in the direction of the phase velocity, the wave ray is distinct and is in the direction of the group velocity (see Figure 3b, c). In the continuum, the wave orthogonals and wave rays coincide. Equations (60) to (62) can be applied to each of the two regions separately by substituting the appropriate values for Δx_1, Δx_2, Δy, γ_{x1} and γ_{x2}. The results are

$$\tan\phi_1 = \frac{(2\cos\gamma_{x1} + 1)\sin\gamma_y}{(2\cos\gamma_y + 1)\sin\gamma_{x1}}, \tag{63}$$

$$\tan\phi_2 = \left(\frac{1}{r}\right)\frac{[(r + 1/r)\cos\gamma_{x2} + 2r - 1/r]\sin\gamma_y}{[(r + 1/r)\cos\gamma_y + 2/r - r]\sin\gamma_{x2}}. \tag{64}$$

The energy flow (governed by equations (61) and (62)) is deflected by the discontinuity at $x = 0$. This is illustrated in Figure 3c which shows a wave front of energy (rather than phase) being refracted. The width of the ray tube is reduced from PR to QS. From the geometry of the figure, if $PR = 1$ then $QS = \cos\phi_2/\cos\phi_1$.

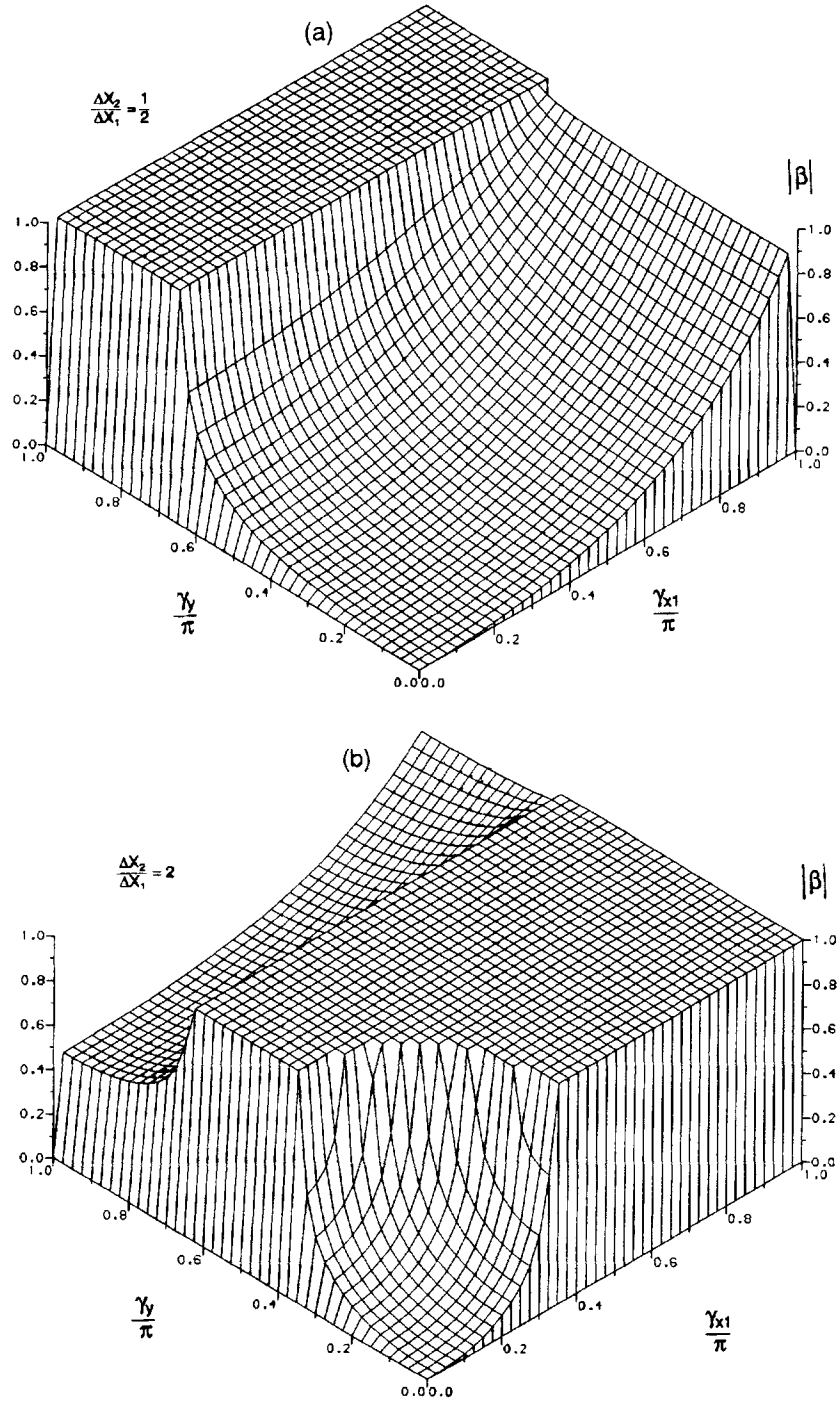

Figure 4. Magnitude of the reflection coefficient for mesh size ratios (a) $\Delta x_2/\Delta x_1 = 1/2$ and (b) $\Delta x_2/\Delta x_1 = 2$

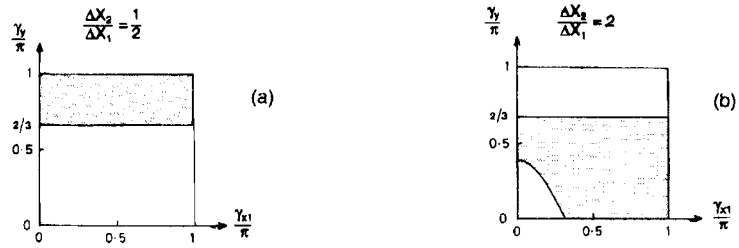

Figure 5. Domains of the dimensionless wavenumbers (γ_{x1}, γ_y) for which total internal reflection occurs (shown shaded) for the mesh size ratios:- (a) $\Delta x_2/\Delta x_1 = 1/2$ and (b) $\Delta x_2/\Delta x_1 = 2$

The total energy per unit surface area (or energy density), E is given by

$$E = \frac{1}{2}\rho g a^2, \tag{65}$$

where ρ is the density of the fluid, g is acceleration due to gravity and a is the wave amplitude. The wave energy flux (F), through a ray tube of width w in the direction of the group velocity vector, is given by

$$F = Ec_g w \tag{66}$$

$$= \frac{1}{2}\rho g a^2 c_g w. \tag{67}$$

From Figure 3 the net energy flux towards the junction (F_{net}) due to the presence of the incident, reflected and transmitted waves is:

$$F_{\text{net}} = F_{\text{inc}} - F_{\text{ref}} - F_{\text{trans}}$$

$$= \frac{1}{2}\rho g 1^2 c_{g1} - \frac{1}{2}\rho g \beta^2 c_{g1} - \frac{1}{2}\rho g \tau^2 c_{g2}\left(\frac{\cos\phi_2}{\cos\phi_1}\right) \tag{68}$$

Substituting equations (37), (45) and (61) (with the appropriate parameters for the two regions) into equation (68) shows that F_{net} is zero and hence energy is conserved across the interface.

When TIR occurs, β and τ are complex. Equation (68) is still valid except that now $|\beta|$ must be used in place of β and similarly for τ. Under these conditions $|\beta| = 1$ and it is easily seen from equation (68) that energy is conserved when there is no energy flux associated with the evanescent transmitted wave. This result is the same as for the 1D case.[3]

4.6. Numerical experiments

A series of 20 numerical experiments were performed to check the results of the analysis. The conditions varied were the incident wavelength ($L_1 = 2\pi/\sigma_1$), the wave approach angle (θ_1) and the mesh expansion or contraction ratio in the x-direction ($\Delta x_2/\Delta x_1$). Six tests were selected for display. The input data is contained in Table I and in all tests, the following values were adopted: $\Delta x_1 = \Delta y = 1\text{m}$, $c = 5$ m/s and $\Delta t = 0{\cdot}2\text{s}$ (or $C_1 = 1$ and $C_2 = 1/r$).

The damping factor in Table 1 refers to the spatial damping of the transmitted wave when TIR occurs (see equation (59)). All tests were 'hot started'. That is, the analytical solutions from equations (33) and (35) were used to prescribe the initial conditions for the FE wave model. The wave model was then run and the residual or difference between the computed solution and the analytical solution was plotted along a transect at right angles to the interface. Any mismatch between the computed solution

Table I. Data for numerical experiments

Test No.	L_1 (m)	L_2 (m)	$\frac{\Delta x_2}{\Delta x_1}$	θ_1	θ_2	β	τ	Damping Factor	γ_{x2}
1	2	2·88	1/2	30°	46·0°	−0·71	0·29	0	0·241 π
2	4	4·00	2	0°	0°	$-1{\cdot}e^{-1{\cdot}23}$	$1{\cdot}15e^{0{\cdot}96}$	$e^{-1{\cdot}76j}$	$\pi-1{\cdot}76i$
3	4	3·58	2	30°	26·6°	$-1{\cdot}e^{-1{\cdot}35}$	$1{\cdot}25e^{0{\cdot}90}$	$e^{-2{\cdot}06j}$	$\pi-2{\cdot}06i$
4	4	4·32	1/2	30°	32·7°	0·12	0·88	0	0·195 π
5	8	7·28	2	30°	27·0°	0·16	1·16	0	0·490 π
6	8	7·39	2	45°	40·8°	0·14	1·14	0	0·410 π

and the analytical solution is soon apparent as a (non-zero) disturbance in the residual. Such a disturbance would emanate from the interface and expand in both the upstream and downstream directions from the first time step onwards. Note that TIR is predicted in Tests 2 and 3. It should be noted that in the experiments, no special internal boundary equations were applied across the interface but the governing FE equations applied throughout the domain. Any reflections from external boundaries were able to be excluded from the results due to the remoteness of the external boundaries from the area of interest.

The experimental procedure was as follows:

- Parameters needed for the initial conditions were calculated.
  Specify: L_1, θ_1 and Δx_2
  Calculate: $\sigma_1 = 2\pi/L_1$, $(\sigma_{x1}, \sigma_y) = (\sigma_1 \cos\theta_1, \sigma_1 \sin\theta_1)$, $(\gamma_{x1}, \gamma_{y1}) = (\sigma_{x1}\Delta x_1, \sigma_y \Delta y_1)$, ω from equation (30), γ_{x2} from equation (42), (β, τ) from equations (44) and (45) or equations (56) and (57) if TIR occurs, γ_2 and L_2 from Snell's law and $\gamma_{x2} = \sigma_2 \Delta x_2 \cos\theta_2$
- Calculate the initial conditions from equations (33) and (35).
- Run the model and check for any discrepancy between the computed solution and the analytical solution.

4.7. Results and conclusions

The experimental results from the wave model are presented in Figures 6 to 11. For each test, there is (a) an oblique view of the 2D wave field as it passes across the interface between the two regions and (b) a 1D transect parallel to the x-axis, showing the variation in the variable η after a number of time steps. The conclusions from the analysis and the numerical experiments are:

- In all cases, the results show that the analytical solution is valid since the residuals in each transect remain zero. (In Figures 6b to 11b, the residuals are represented by small triangles). That is, the analytical solution was 'held' by the model. (It should be commented that in Figure 8 it appears that the transmitted wave is moving parallel to the x-axis. This is not the case however and is a consequence of the graphics package representing the very small amplitude of the spatially damped, transmitted wave.)
- The longer the incident wavelength relative to the nodal spacings in both regions, the more transparent is the incident wave to mesh discretisation. As the incident wavelength is increased, the amplitude of the (spurious) reflected wave is reduced, and the closer the transmitted wave amplitude is to unity. The degree of spurious numerical refraction is reduced at the longer wavelength end of the spectrum.
- TIR occurs when $\cos\gamma_{x2}$ exceeds unity and γ_{x2} is complex. If $\gamma_{x2} = \pi + i\cosh^{-1}(-R)$, then the transmitted wave has a $2\Delta x_2$ wavelength in the x-direction. (If $\gamma_{x2} = 0 - i\cosh^{-1}(R)$, the transmitted wave would have an infinitely long wavelength in the x-direction.)

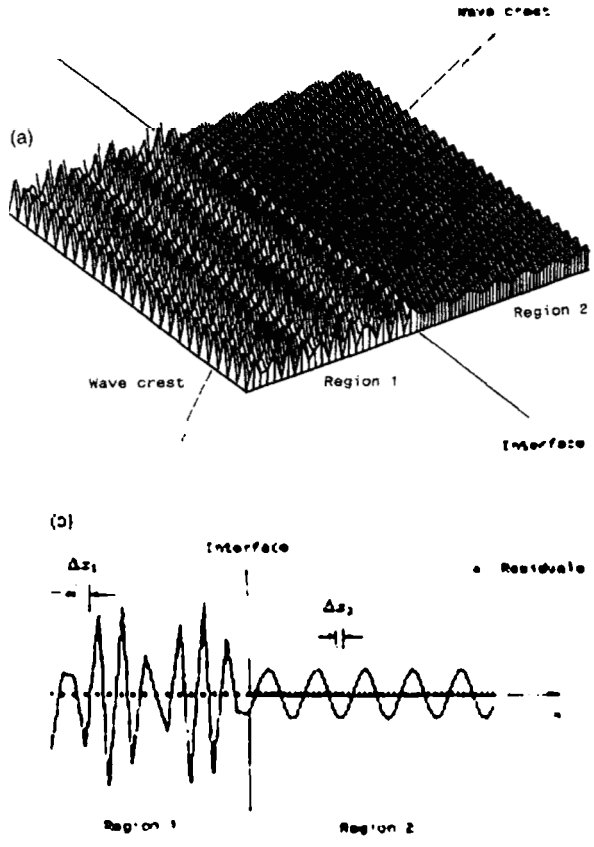

Figure 6. Test No. 1-(a) perspective view and (b) transect parallel to x-axis

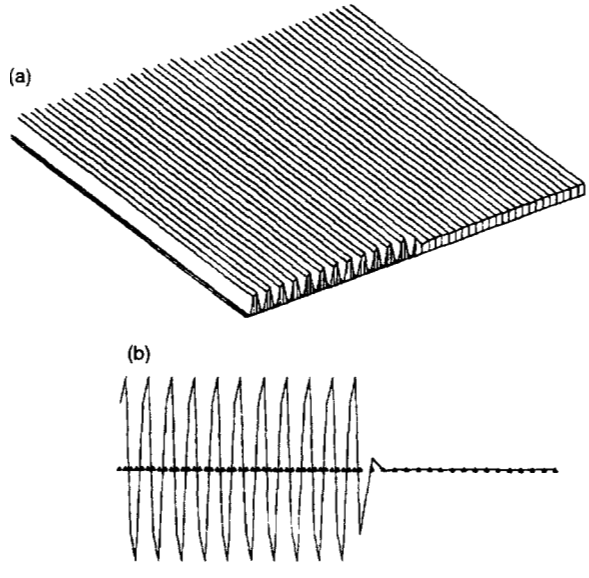

Figure 7. Test No. 2-(a) perspective view and (b) transect parallel to x axis

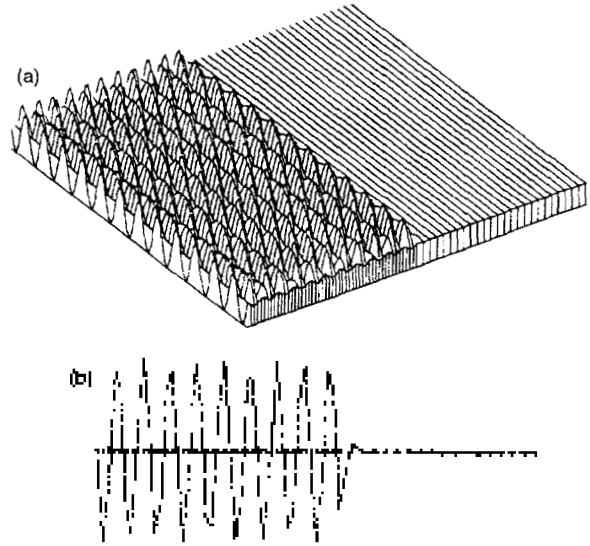

Figure 8. Test No. 3-(a) perspective view and (b) transect parallel to x-axis.

- Factors affecting the occurrence of TIR include the incident wavelength and approach angle as well as the mesh size change. TIR can occur for both mesh expansion and mesh contraction.
- Energy flux across the interface is conserved. When TIR occurs, the same amount of energy transported towards the interface by the incident wave is also transported back by the reflected wave. In these circumstances, there is no energy flux associated with the evanescent transmitted wave.
- The rate of spatial damping of the transmitted wave which occurs when there is TIR, can be rapid. For example, in Test No. 2 the damping factor was e^{-1763y}. Therefore at one, two and three nodes

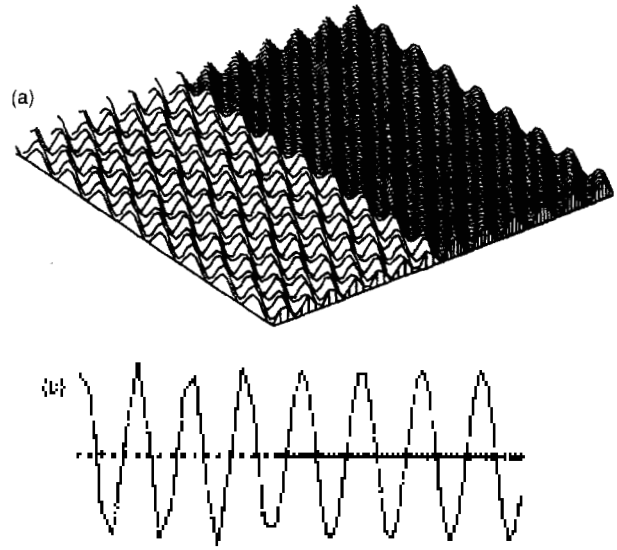

Figure 9. Test No. 4-(a) perspective view and (b) transect parallel to x-axis.

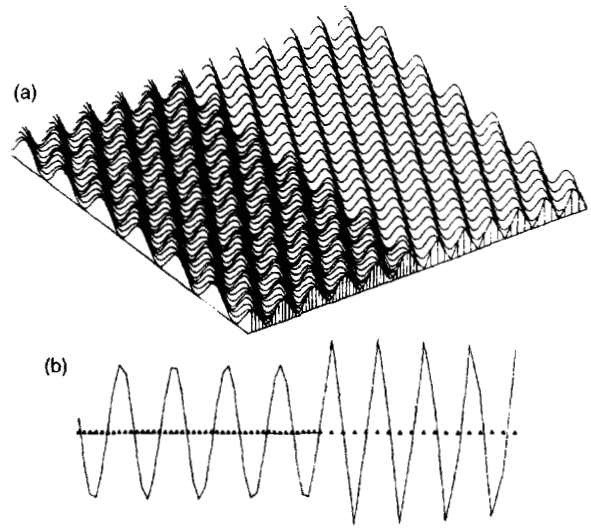

Figure 10. Test No. 5–(a) perspective view and (b) transect parallel to x-axis

downstream of the interface in the x-direction (i.e. $j = 1, 2$ and 3), the amplitude of the transmitted wave is reduced from $|\tau|$ at the interface to $0{\cdot}172\ |\tau|$, $0{\cdot}03\,|\tau|$ and $0{\cdot}0050\,|\tau|$ respectively.

- Factors affecting the occurrence and degree of spurious reflection and refraction occurring in wave models will depend upon:
  - ⋆ their formulation (i.e. whether they are based upon the shallow water equations or the second order wave equation as well as the particular numerical algorithm used to discretise the governing equations),
  - ⋆ the incident wavelength,
  - ⋆ changes in mesh size, and
  - ⋆ the approach angle.

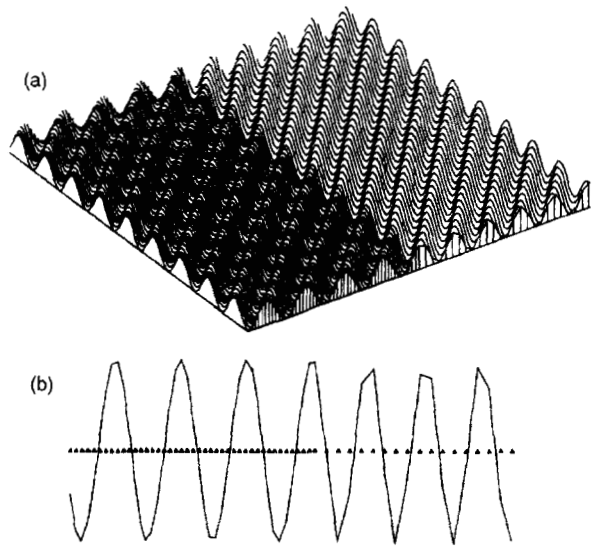

Figure 11. Test No. 6–(a) perspective view and (b) transect parallel to x-axis

- In wave models with non-uniform meshes, spurious refraction and reflection will be occurring throughout. Such effects can be minimised by ensuring that the most important wavelengths are well resolved by the mesh.

ACKNOWLEDGEMENT

We thank Robin Brech for her skilled drafting and the reviewers for their suggestions for clarifying the paper.

REFERENCES

1. Z. P. Bazant, Spurious reflection of elastic waves in non-uniform finite element grids, *Comput. Methods Appl. Mech. Eng.*, **16**, 91–100 (1978).
2. Z. P. Bazant and Z. Celep, Spurious reflections of elastic waves in non–uniform meshes of constant and linear strain FE, *Comp. Structures*, **15**, 451–459 (1982).
3. B. Cathers, S. Bates and B.A. O'Connor, Internal wave reflections and transmissions arising from a non-uniform mesh. Part III: the occurrence of evanescent waves in the Crank–Nicolson linear finite element scheme, *Int. j. numer. methods fluids*, **9**, 833–853 (1989).
4. B. Cathers and B. A. O'Connor, The group velocity of some numerical schemes, *Int. j. numer. methods fluids*, **5**, 201–224, (1985).
5. M. G. G. Foreman, An analysis of two-step time discretizations in the solution of the linearized shallow water equations, *J. Comput. Phys.*, 51, 454–483 (1983).
6. C. P. Kentzer, Group velocity and propagation of numerical errors, *AIAA Paper No. 72–153*, AIAA 10th Aerospace Sciences Meeting, San Diego, California, Jan. 17–19 (1972).
7. L. N. Trefethen, Wave propagation and stability for finite difference schemes, Ph.D. Thesis, Stanford University, May 1982; also Department of Computer Science Report No. STAN-CS-82-905, 1982.
8. R. Vichnevetsky, Fourier Analysis of Numerical Approximations of Hyperbolic Equations, *SIAM Studies in Applied Mathematics*, 1982.
9. R. Vichnevetsky, Invariance theorems concerning reflection at numerical boundaries, *J. Comput. Phys.*, **63**, 268–282 (1986).
10. R. Vichnevetsky, Wave propagation analysis of difference schemes for hyperbolic equations: a review, *Int. j. numer. methods fluids*, 7, 409–452 (1987).